

# Nanoscale

Accepted Manuscript



This is an *Accepted Manuscript*, which has been through the Royal Society of Chemistry peer review process and has been accepted for publication.

*Accepted Manuscripts* are published online shortly after acceptance, before technical editing, formatting and proof reading. Using this free service, authors can make their results available to the community, in citable form, before we publish the edited article. We will replace this *Accepted Manuscript* with the edited and formatted *Advance Article* as soon as it is available.

You can find more information about *Accepted Manuscripts* in the [Information for Authors](#).

Please note that technical editing may introduce minor changes to the text and/or graphics, which may alter content. The journal's standard [Terms & Conditions](#) and the [Ethical guidelines](#) still apply. In no event shall the Royal Society of Chemistry be held responsible for any errors or omissions in this *Accepted Manuscript* or any consequences arising from the use of any information it contains.

## A Hybrid Enrichment Process Combining Conjugated Polymer Extraction and Silica Gel Adsorption for High Purity Semiconducting Single-Walled Carbon Nanotubes (SWCNT)

Jianfu Ding\*<sup>1</sup>, Zhao Li<sup>1</sup>, Jacques Lefebvre<sup>2</sup>, Fuyong Cheng<sup>3</sup>, Jeffrey L. Dunford<sup>2</sup>,  
Patrick R. L. Malenfant\*<sup>2</sup>, Jefford Humes<sup>4</sup>, Jens Kroeger<sup>4</sup>

<sup>1-3</sup> Security and Disruptive Technologies Portfolio, National Research Council Canada, <sup>1</sup>M-12 and <sup>2</sup>M-50, 1200 Montreal Road, Ottawa, Ontario, K1A 0R6, Canada. <sup>3</sup>100 Sussex Dr, Ottawa, Ontario K1A 0R6. <sup>4</sup>Raymor Industries Inc. 3765 La Vérendrye, Boisbriand, Québec, J7H 1R8, Canada

### Abstract:

A novel purification process for the enrichment of sc-SWCNTs that combines selective conjugated polymer extraction (CPE) with selective adsorption using silica gel, termed hybrid-CPE (h-CPE), has been developed, providing a high purity sc-SWCNT material with a significant improvement in process efficiency and yield. Using the h-CPE protocol, a greater than 5 fold improvement in yield can be obtained compared to traditional CPE while obtaining sc-SWCNT with a purity >99.9% as assessed by absorption spectroscopy and Raman mapping. Thin film transistor devices using the h-CPE derived sc-SWCNTs as the semiconductor possess mobility values ranging from 10-30 cm<sup>2</sup>V<sup>-1</sup>s<sup>-1</sup> and current on/off ratio of 10<sup>4</sup>-10<sup>5</sup> for channel lengths between 2.5 and 20 μm.

### Introduction

Single walled carbon nanotubes (SWCNT) are unique building blocks in electronics and are a key enabling material for flexible and printed electronics.<sup>1-4</sup> High purity semiconducting SWCNT (sc-SWCNT) will enable fully printed transistors and circuits with the required performance to support low-cost/large-area sensor arrays and flexible electrophoretic displays as well as flexible OLED display drivers.<sup>5-12</sup> Several methods have been used to isolate high purity metallic SWCNT (m-SWCNT) and sc-SWCNTs such as density gradient ultracentrifugation (DGU), gel-based chromatography and aqueous two phase extraction (ATPE).<sup>13-20</sup> Recent developments with ATPE have provided much insight into the solution behavior of SWCNTs demonstrating many elegant

examples of SWCNT enrichment.<sup>18-20</sup> Another effective technique to isolate sc-SWCNTs is conjugated polymer extraction (CPE), which was first demonstrated by Nicholas and co-workers.<sup>21</sup> Similar to aqueous based techniques (*vide supra*) this approach provides sc-SWCNT with semiconducting purity levels higher than 99% and excellent thin film transistor (TFT) performance.<sup>22-27</sup> In addition, recent developments have shown that self-assembled polymers bearing  $\pi$ -conjugated moieties are also effective at sc-SWCNT enrichment, yet provide a means of easily decomposing the polymer to release the enriched sc-SWCNTs.<sup>28-29</sup>

In the CPE process, sc-SWCNTs are selectively dispersed with conjugated polymers in an organic solvent, typically non-polar aromatic, whereby m-SWCNT are largely found in the sediment after centrifugation with low centrifugal force. Currently the CPE process suffers from low efficiency and yield and repeated extractions are typically used to promote the yield at the expense of purity.<sup>22</sup> The method currently stands to benefit from improvements in process efficiency and yield yet retain the scalability and high purity the CPE platform provides. Herein, we report a novel hybrid CPE (h-CPE) process for the enrichment of sc-SWCNTs, in which silica gel is used to combine selective extraction with selective adsorption providing a high purity material with a significant improvement in process efficiency and yield (see Figure 1).

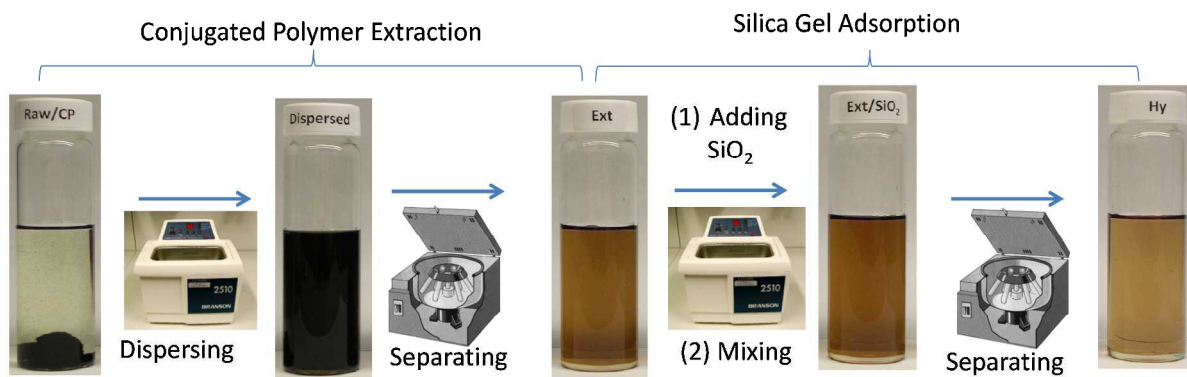


**Figure 1.** h-CPE process for sc-SWCNT enrichment combining conjugated polymer extraction and silica gel adsorption.

While the CPE enrichment mechanism is not currently fully understood, experimental evidence suggests that the selectivity may arise from the fact that bundles containing m-SWCNT are more difficult to exfoliate and dispersed m-SWCNT have a higher propensity to reform bundles and aggregate due to their higher polarizability, enabling a facile separation from sc-SWCNT via low g centrifugation. The extent to which the semiconducting purity and the yield can be enhanced depends on the colloidal stability (energetics) of the SWCNT-polymer complex, which can be adjusted by matching the polymer structure with SWCNT diameter/chirality and varying the solvent, concentration, polymer-SWCNT ratio, conjugated repeat units in the main chain of the conjugated polymer as well as the length of the polymer side chains. Usually when using CPE, a high semiconducting purity can be obtained when a low polymer/SWCNT ratio is used, but a low yield will result.<sup>22-27</sup> Higher polymer/SWCNT ratios will increase the yield at the expense of purity.<sup>22</sup> Using the h-CPE protocol a 5 fold improvement in yield can be obtained in which a single adsorption step provides up to 90% yield with sc-SWCNT purity >99.9%, as assessed by absorption spectroscopy and Raman mapping. Thin film transistor devices with channels using h-CPE process derived sc-SWCNTs as the semiconductor have mobility values ranging from 10-30 cm<sup>2</sup>V<sup>-1</sup>s<sup>-1</sup> and current on/off ratio of 10<sup>4</sup>-10<sup>5</sup> consistent with the CPE method of enrichment.

## Experimental Section

**Materials.** Purified plasma SWCNT (RN-000, from Raymor Nanotech) and poly(9,9-di-n-dodecylfluorene) (PFDD) with a number average molecular weight of 17.6 kDa and polydispersity index of 3.89 were used.<sup>22</sup> Silica gel (60A, 230-400 mesh) obtained from Rose Sci. Ltd was used as received.

**Enrichment.** PFDD extraction: 25 mg of purified plasma SWCNT sample was first conditioned in a PFDD/toluene solution to reduce batch to batch fluctuation. Conditioning was done by sonicating the sample in 25 mL of PFDD/toluene solution (1 mg/mL) for 30 min using a tip sonicator (Branson sonifier 250, micro-tip,  $\phi$ 5 mm, cycle 60% and output 30%) followed by centrifugation at

12,500 rpm using an SS-34 rotor (RCF 18,690) for 30 min. This process was applied again to the obtained sediment by using 50 mL of PFDD/toluene solution (1 mg/mL). The supernatant was collected as Sample Ex1. The resulting sediment was extracted once more in 50 mL of PFDD/toluene solution (4 mg/mL) to collect the supernatant (Ex2). Meanwhile, another conditioned sample was extracted in 50 mL of PFDD/toluene solution (0.5 mg/mL) to obtain the control sample (Ex1a). See Figure S1 for a process schematic.

**Adsorption treatment.** 25 and 50 mg of silica gel was added into Ex1 and Ex2 (the SiO<sub>2</sub>/SWCNT weight ratio was calculated based on the UV absorption (938 nm) being 29 and 18 respectively). The mixtures were sonicated in a bath sonicator (Branson 2510) for 40 min, followed by standing for 3 h, and then centrifuged at 12,500 rpm using SS-34 rotor (RCF 18,690) for 30 min. The supernatants (Hy1 and Hy2) were collected and characterized. The sediment was rinsed with 2 mL of methanol and soaked in 2 mL of 50% HF solution to dissolve the SiO<sub>2</sub>. The liquid phase was removed after 5 min and the solid was rinsed with 25 mL of water three times and then 25 mL of methanol once. The solid was dried under vacuum at room temperature and re-dispersed in 2 mL of toluene to obtain dispersions of the adsorbed materials (Ad1 and Ad2).

**Characterization.** Absorption spectra were collected on a UV-Vis-NIR spectrophotometer (Cary 5000, Varian) over a wavelength range from 300 to 2100 nm. A double beam mode was used with a pure solvent cuvette placed in the reference channel. The yield of the enrichment processes and the purity of the SWCNT materials were determined from the absorption spectra based on a previously reported method.<sup>22</sup> Raman spectra were acquired with an InVia Raman microscope (Renishaw) from drop-cast samples. 514 nm (2.41 eV), 633 nm (1.96 eV) and 785 nm (1.58 eV) laser excitation sources and 50× magnification objective lens were used. Spectra were recorded from 100–3000 cm<sup>-1</sup>, with a resolution of 4 cm<sup>-1</sup>. Raman mapping images were collected using a 100× magnification objective lens with a laser spot size of ~ 1 μm<sup>2</sup> and step size of 1 μm in both X and Y directions in a 31 x 31 = 961 μm<sup>2</sup> area.<sup>30</sup> Tube density was calculated from a calibration curve based on the averaged intensity at the G<sup>+</sup> 1592 cm<sup>-1</sup> peak.<sup>30</sup> Ten areas were examined, from which the purity was

statistically evaluated. Photoluminescence excitation maps (PLE) were acquired using a custom-built system with a Ti-sapphire laser as the excitation source and InGaAs photodiode array for detection (extended sensitivity between 900 and 2100 nm).<sup>22</sup> Spectra were obtained from solutions in capillaries with a rectangular cross-section and 100 mm path length. For the polymer wrapping density studies, fluorescence spectra were recorded on a Perkin-Elmer LS 55 luminescence spectrometer excited at 385 nm. The peak intensity at  $\sim 420$  nm was used to determine the PFDD concentration. TFT devices were prepared using commercial OFET substrates (Fraunhofer IPMS) with 2.5, 5, 10 and 20  $\mu\text{m}$  channel lengths, 230 nm  $\text{SiO}_2$  dielectric, and a common bottom gate (n-doped Si), bottom contact (Ti/Au) configuration with interdigitated source/drain electrodes having a 2000  $\mu\text{m}$  channel width. Devices were prepared and characterized as reported previously.<sup>22, 30</sup>

## Results & Discussion

Plasma torch-grown SWCNTs were used to develop the h-CPE process. These SWCNTs have a relatively large diameter centered at about 1.3 nm and low surface defect density.<sup>31</sup> Typically the adsorption treatment involves adding silica gel at a  $\text{SiO}_2/\text{sc-SWCNTs}$  weight ratio of  $\sim 20$  (see experimental) to the enriched supernatant obtained from a PFDD extraction (e.g. Ex1 and Ex2). The mixtures are sonicated, allowed to stand for 3 h to equilibrate the adsorption of m-SWCNTs on the silica gel followed by low g centrifugation to efficiently isolate sc-SWCNTs in high yield. The adsorption process is illustrated in Figure 2.

To assess the effectiveness of the adsorption step, two sc-SWCNTs solutions with different semiconducting purities were generated from the same stock sample: a relatively high purity sample with a  $\phi$  value of 0.404 and a relatively lower purity sample with a  $\phi$  value 0.356 (see refs 22 and 30 for details regarding the semiconducting purity figure of merit  $\phi$ ). They were prepared by a successive PFDD extraction in toluene at a SWCNT concentration of 0.5 mg/mL and PFDD/SWCNT ratio of 2/1 (Ex1) followed by 8/1 (Ex2). A control sample (Ex1a) with a  $\phi$  value of

0.422 was also prepared using PFDD extraction at conditions optimized for a high semiconducting purity (SWCNT concentration of 0.5 mg/mL and PFDD/SWCNT ratio of 1/1).<sup>22</sup>

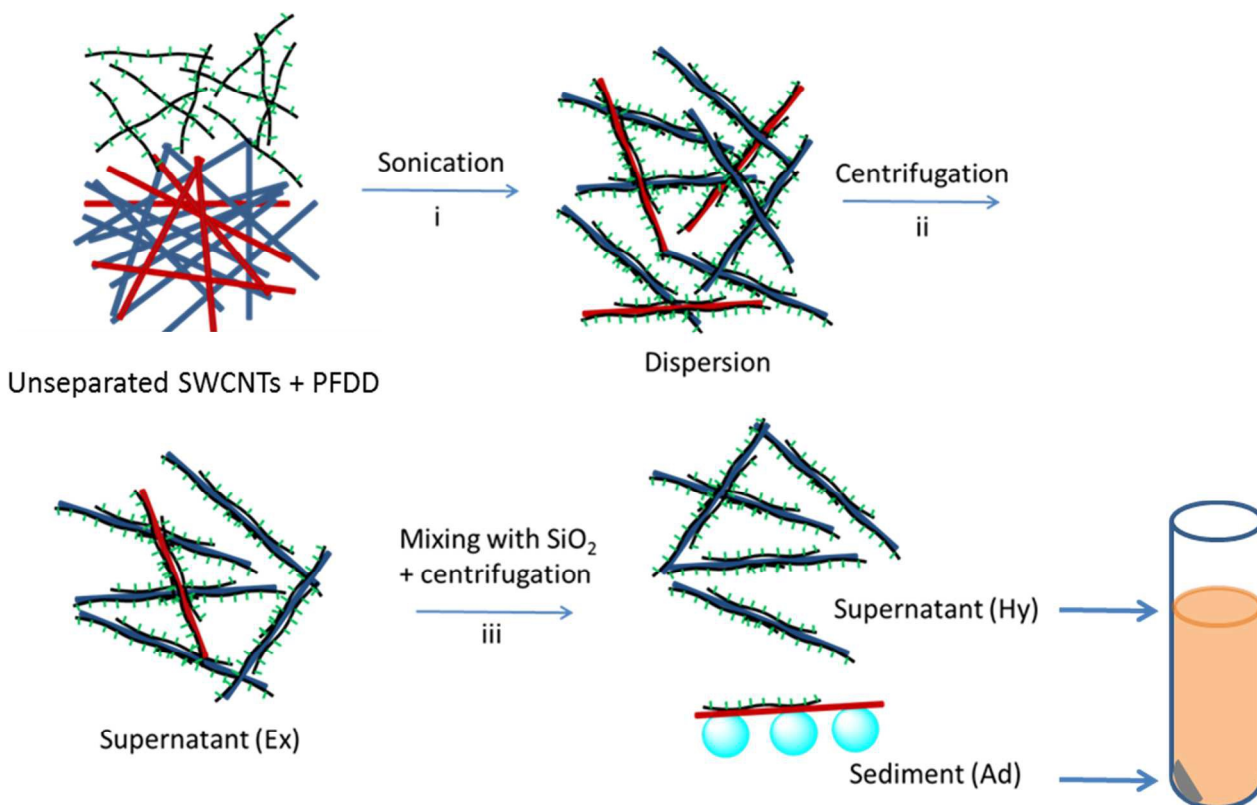


**Figure 2.** Graphical depiction of h-CPE process for sc-SWCNT enrichment (i) PFDD dispersion (ii) CPE enrichment producing Ex sample, (iii) silica gel adsorption producing Hy and Ad samples. Red = m-SWCNT, Blue = sc-SWCNT, Black/Green = PFDD, Cyan spheres = SiO<sub>2</sub> particles.

The absorption spectra of the unseparated SWCNTs and enriched samples (Ex1a, Ex1, Ex2) can be seen in Figure 3. The yield and  $\phi$  value for each sample are also indicated in the inset. As expected, the yield of the control extraction (Ex1a) is low at 1.5% due to its low PFDD/SWCNT ratio (1/1). Yield increased to 3.4% (Ex1) and 11% (Ex2) as the PFDD/SWCNT ratio increased to 2/1 and 8/1, respectively. The corresponding  $\phi$  value decreased from 0.422 for Ex1a to 0.404 for Ex1 and 0.356 for Ex2, consistent with lower purity as a function of higher PFDD/SWCNT ratio.

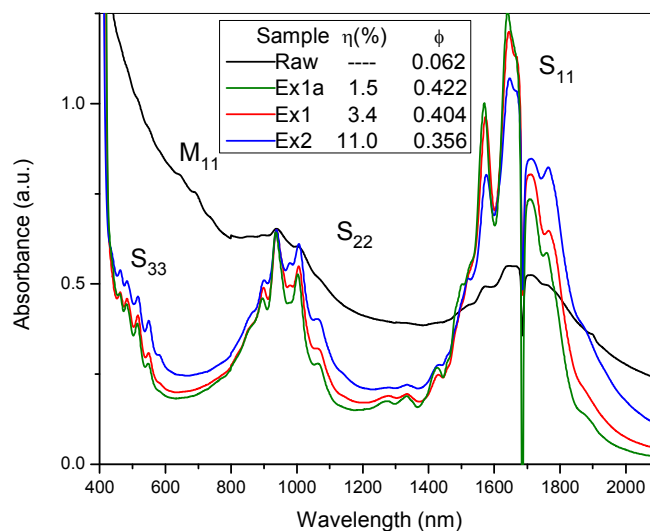


**Figure 3.** Absorption spectra of the unseparated (raw) plasma SWCNT sample and the supernatants from the extractions using PFDD/SWCNT ratios of 1:1 (Ex1a), 2:1 (Ex1) and 8:1 (Ex2). Yields ( $\eta\%$ ) are calculated based on the weight of unseparated SWCNT samples.

Due to the high purity of Ex1a, an additional adsorption treatment to this sample does not improve the purity ( $\phi$  value unchanged). However, an adsorption treatment effected on samples Ex1 and Ex2 produced higher semiconducting purity samples, as indicated by their absorption spectra displayed in Figure 4. After the adsorption step, samples Hy1 and Hy2 have measurably lower absorption intensities between 600 and 800 nm, where the M11 m-SWCNT absorption band is located. The  $\phi$  values increased from 0.404 to 0.416 for Hy1 and from 0.356 to 0.413 for Hy2 as indicated in the inset of Figure 4. These two  $\phi$  values are comparable to that of control sample Ex1a (0.422), confirming a similarly high semiconducting purity, yet the overall yields for the h-CPE process are higher (3.0% for Hy1 and 10.0% Hy2), given higher PFDD/SWCNT ratios were used initially and the yield of the adsorption step is typically 80-90% (see Figure S2 - for  $\phi$  and yield data as a function of  $\text{SiO}_2/\text{SWCNT}$ ). It is important to note that successive extractions in the absence of  $\text{SiO}_2$  do not provide the same purity and yield performance as obtained with the h-CPE process.<sup>22</sup> The

chirality distribution for Ex and Hy samples are indistinguishable (see Figure S3 for PLE maps). The selective removal of m-SWCNTs by the adsorption step is further confirmed by the UV spectrum of the materials adsorbed onto the silica gel (Ad1 and Ad2). These materials were isolated from silica gel by using a 50% Hydrogen Fluoride solution to etch away the silica gel. Absorption spectra for Ad1 and Ad2 display much higher background absorbance intensity between 600-800 nm, consistent with the material adsorbed on silica gel being significantly less pure than the material found in the supernatant.

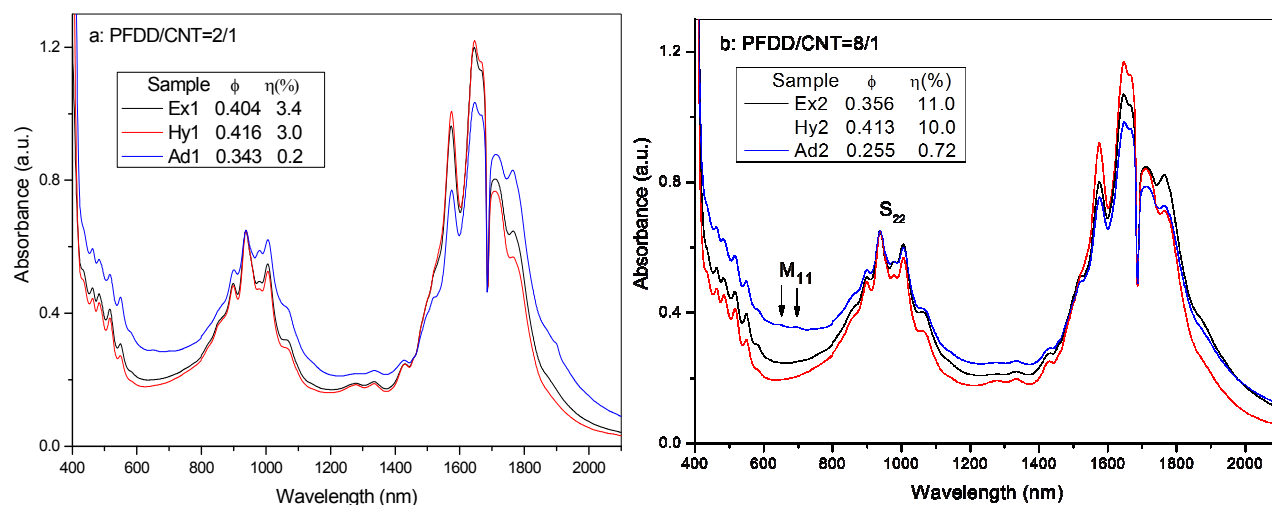


**Figure 4.** Absorption spectra of sc-SWCNT enriched supernatant from PFDD extraction (Ex), the resulting supernatants from the adsorption step (Hy), and the materials adsorbed onto the silica gel (Ad) at PFDD/SWCNT ratios of (a) 2/1 and (b) 8/1. Yields ( $\eta\%$ ) are calculated based on the weight of raw SWCNT samples.

The semiconducting purity was further examined by Raman spectroscopy. Figure 5 displays spectra of the D and G bands under 633 nm (1.96 eV) laser excitation and the radial breathing mode (RBM) under 785 nm (1.58 eV) laser excitation for Ex, Hy and Ad samples (2/1 and 8/1 PFDD/CNT ratio). The G band displays three features:  $G^-_m$ ,  $G^-_{sc}$ , and  $G^+$ . The  $G^-_m$  peak with a broad Breit-Wigner-Fano (BWF) line shape is associated with m-SWCNTs while the narrow  $G^-_{sc}$  and  $G^+$  with a Lorentzian line shape are associated with sc-SWCNTs.<sup>30</sup> Comparing the relative

intensity of  $G_m^-$  with  $G^+$ , we can estimate the relative concentration of the m-SWCNTs in the samples as represented by a figure of merit.<sup>32</sup> Figures 5a1 and 5a2 have a weak  $G_m^-$  shoulder for Ex1 and Ex2 consistent with enriched sc-SWCNT, yet this shoulder is completely absent for the samples that underwent the adsorption treatment (Hy1 and Hy2). It is important to note that the  $\phi$  value changed negligibly after the adsorption step was performed on sample Ex1, yet there is a significant improvement in the purity as assessed by the  $G_m^-$ ; consistent with a strong driving force to adhere m-SWCNTs impurities onto the silica gel. Furthermore, the large capacity to bind m-SWCNT impurities is evidenced with the effectiveness of the adsorption process leading to Hy2, which appears to be as pure as Hy1 (and Ex1a) even though the much less pure Ex2 feedstock was used. As expected, the materials adsorbed on silica gel (Ad1 and Ad2) showed a much stronger  $G_m^-$  peak, consistent with m-SWCNTs accumulating on the silica gel surface. The same conclusion can be drawn from the RBM data in Figure 5b, where the bands in the shaded area are associated with m-SWCNTs. It can be seen that the broad bands in the shaded area centered at  $157\text{ cm}^{-1}$  are completely eliminated after the adsorption treatment, while this band increased significantly in intensity for the materials adsorbed on the silica gel (Ad1 and Ad2).

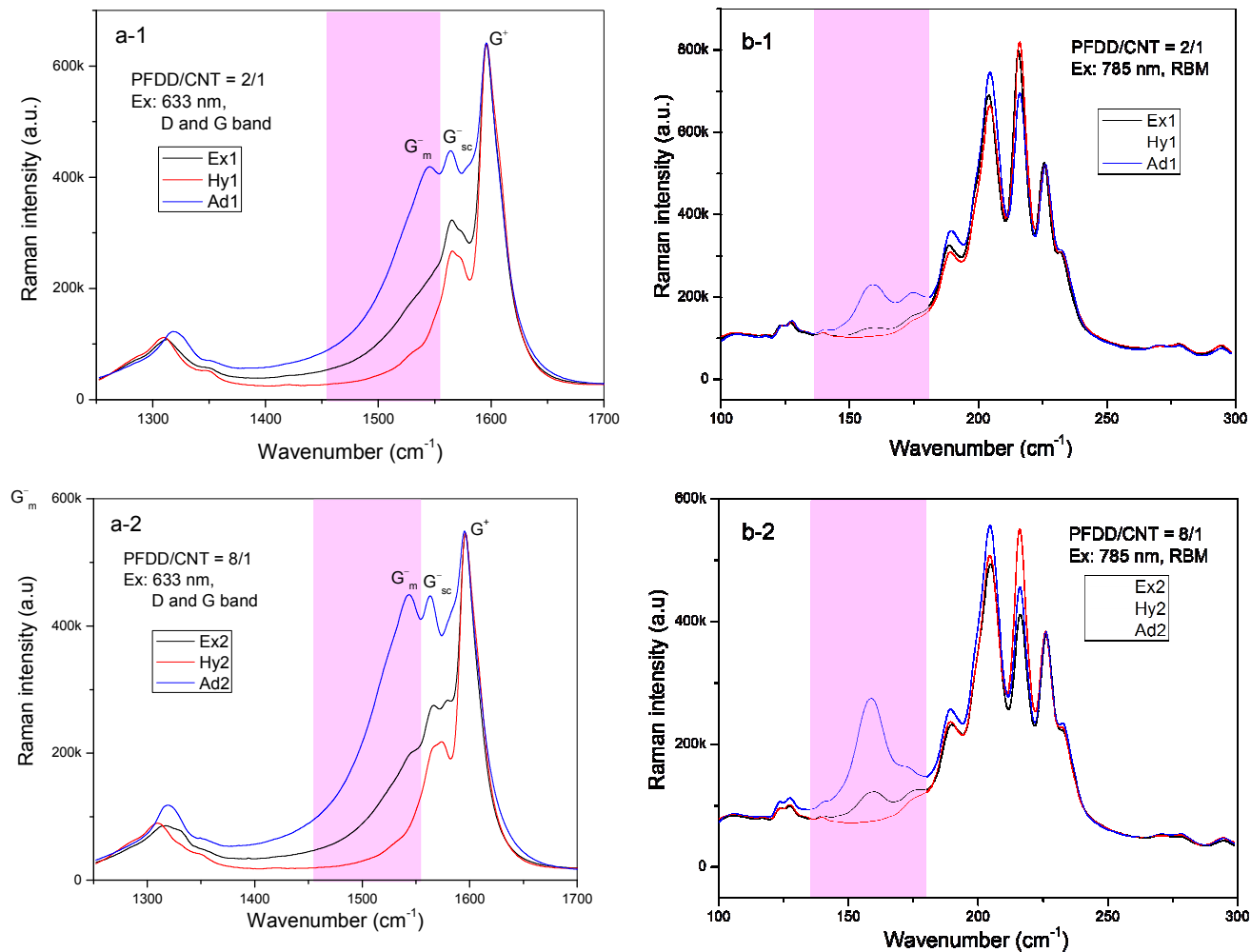


**Figure 5.** Raman spectra of the sc-SWCNT enriched sample from the PFDD extraction (Ex), from the h-CEP (Hy) and the materials adsorbed onto the silica gel (Ad) at PFDD/SWCNT ratios of (1) 2/1 and (2) 8/1 at excitation wavelengths of (a) 633 nm and (b) 785 nm. Data for Ex1a is comparable to Hy1 and Hy2 (not shown).

The semiconducting purity improvement resulting from the adsorption treatment was further evaluated by Raman mapping, where the maps were plotted based on the Raman intensity of the  $G_m^-$  band at  $1545\text{ cm}^{-1}$  for a  $31 \times 31 = 961\text{ }\mu\text{m}^2$  area. This method enables m-SWCNT counting and

provides more granularity to assess the semiconducting purity, the details of the method have already been reported elsewhere.<sup>30</sup>

We scanned 10 areas and found the m-SWCNT count to range from 6 to 17 m-SWCNTs. The tube density in the examined areas was determined to be 16 tubes/ $\mu\text{m}^2$  for Hy2, calculated from the averaged  $G^+$  peak intensity excited by 514 nm laser.<sup>30</sup> Hence the m-SWCNT content is calculated to be  $0.07\pm 0.02\%$ ; i.e. the sc-purity is  $99.93\pm 0.02\%$ . Similarly, the m-SWCNT content of Ex2 and Ad2 samples are estimated to be 1.7% and 8.4%, respectively. This result shows that the adsorption treatment promoted the semiconducting purity from 98.3% (Ex2) to 99.93% (Hy2), and thus reduced m-SWCNT impurity by more than one order of magnitude with excellent yield (see Figure S4 for Raman maps). Such high purities cannot be achieved with successive extractions without substantially lower yields (< 2% vs 10%).<sup>24</sup>

Owing to the high concentration of mobile carriers, m-SWCNTs have a  $10^3\sim 10^5$  larger polarizability compared to sc-SWCNT.<sup>33-34</sup> This difference has been used to rationalize the mechanisms that underpin several sc-SWCNT enrichment techniques such as dielectrophoresis, ATPE, CPE and chromatography.<sup>18-19, 33-36</sup> We believe that under our experimental conditions (low polarity aromatic solvents), the higher polarizability of m-SWCNTs not only leads to bundles that are less susceptible to exfoliation (leading to preferential extraction of sc-SWCNTs during the dispersion step), but the polarizability of m-SWCNTs that are dispersed initially upon sonication will ultimately drive their re-bundling/aggregation as they assemble with defective or doped SWCNTs having polar moieties. This interpretation is consistent with time lapse studies that show an increase in semiconducting purity as a function of time after dispersion prior to centrifugation.<sup>22</sup> The addition of silica gel to a partially enriched solution of sc-SWCNT further exploits this colloidal behavior. While more experimentation is required to elucidate the mechanism, two possible modes of action may be at play during the h-CPE process. The lower dispersability of m-SWCNTs may play a role in which the silica gel effectively adsorbs less stable colloids (re-formed bundles or non-exfoliated bundles) containing m-SWCNT, yet we don't rule out the possibility that well-dispersed metallic SWCNTs may directly adhere to  $\text{SiO}_2$ .

Lastly, the relative purity difference between the samples before and after adsorption treatment (Ex2, Hy2 and Ad2) was further compared by fabricating TFT devices with 2.5  $\mu\text{m}$  and 5.0  $\mu\text{m}$  channel lengths. As expected, Hy2 in a 2.5  $\mu\text{m}$  channel device had the best performance, with mobility values (calculated from transconductance measured in the linear regime) ranging from 10-15  $\text{cm}^2/\text{Vs}$  and current ON/OFF ratios of  $10^4$ - $10^5$  (see Figure S5 for transfer curves). It should be noted that the channel width of the devices is 2000  $\mu\text{m}$ , and with a network density of 16 SWCNTs/ $\mu\text{m}^2$ ,  $\sim 80,000$  SWCNTs are estimated in the channel of a 2.5  $\mu\text{m}$  device. The ON/OFF ratios of 2.5  $\mu\text{m}$  channel devices were dramatically reduced to 77 and 8.0 for the Ex2 (19 SWCNTs/ $\mu\text{m}^2$ ) and Ad2 (8 SWCNTs/ $\mu\text{m}^2$ ), respectively, consistent with higher m-SWCNT impurity of these samples. The ON/OFF ratio data for four devices with a 5.0  $\mu\text{m}$  channel length are compared in Figure 6, showing that ON/OFF ratios of devices from the Hy2 sample were  $> 10^5$ . These values decreased to  $\sim 10^3$  for Ex2 and  $\sim 10^2$  for Ad2. For longer channels ( $L = 10$  and 20  $\mu\text{m}$ ), mobility values of 20-30  $\text{cm}^2/\text{Vs}$  and ON/OFF ratios  $> 10^5$  were typical.<sup>37</sup> All of these results are consistent with the determined purity values (*vide supra*).

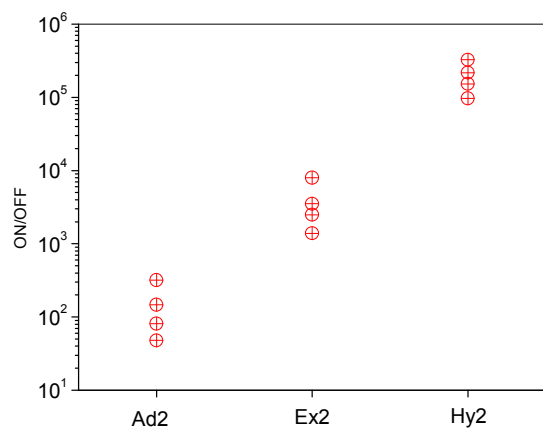


**Figure 6.** Comparison of the current ON/OFF ratio for four devices with  $L = 5.0 \mu\text{m}$  for Ad2, Ex2 and Hy2.

In closing, we have used four indices to validate the sc-purity: the  $\phi$  value from absorption spectra, the intensity ratio of the  $G^-_m$  band at  $1543\text{ cm}^{-1}$  over the  $G^+$  band at  $1592\text{ cm}^{-1}$  ( $G^-/G^+$ ) from Raman scattering at  $633\text{ nm}$  excitation, m-SWCNT counting by Raman mapping, and the current ON/OFF ratio of TFT devices (see Figure S6). The h-CPE process has been demonstrated to provide sc-SWCNTs with metallic impurity levels on the order of a few hundred ppm with a 5 fold improvement in yield compared to traditional CPE. The sc-purity has been quantified to be  $>99.9\%$  using Raman mapping and TFT results show that excellent device performance is achieved with short channels (2.5 and 5.0 microns) even with very large channel widths (2000 microns).

## References

1. Avouris P.; Martel, R. *MRS Bull.* **2010**, *35*, 306-313.
2. Che, Y.; Chen, H.; Gui, H.; Liu, J.; Liu B.; Zhou C. *Semicond. Sci. Technol.* **2014**, *29*, 073001
3. Noh, J.; Jung, M.; Jung, Y.; Yeom, C.; Pyo, M.; Cho, G. *Proc. IEEE*, **2015**, *103*, 554-566.
4. Zaumseil, J. *Semicond. Sci. Technol.* **2015**, *30*, 074001.
5. Lau, P. H.; Takei, K.; Wang, C.; Ju, Y.; Kim, J.; Yu, Z.; Takahashi, T.; Cho, G.; Javey, A. *Nano Lett.* **2013**, *13*, 3864–3869.
6. Kim, B; Jang, S; Geier, M. L.; Prabhumirashi, P. L.; Hersam, M. C.; Dodabalapur, A. *Nano Lett.* **2014**, *14*, 3683–3687.
7. Chen, H; Cao, Y; Zhang, J; Zhou, C. *Nat. Commun.* **2014**, *5*, 4097.
8. Cao, X.; Chen, H.; Gu, X.; Liu, B.; Wang, W.; Cao, Y.; Wu, F.; Zhou, C. *ACS Nano* **2014**, *8*, 12769–12776.
9. Xu, W.; Zhao, J.; Qian, L.; Han, X.; Wu, L.; Wu, W.; Song, M.; Zhou, L.; Su, W.; Wang, C.; Nie, S.; Cui, Z. *Nanoscale* **2014**, *6*, 1589-1595.
10. Jung, M.; Kim, J.; Koo, H.; Lee, W.; Subramanian, V.; Cho, G. *Journal of Nanoscience and Nanotechnology* **2014**, *14*, 1303-1317.
11. Jung, M. H.; Kim, J.; Noh, J.; Lim, N.; Lim, C.; Lee, G.; Kim, J.; Kang, H.; Jung, K.; Leonard, A.; Tour, J. M.; Cho, G. *IEEE Trans. Elec.* **2010**, *57*, 571–580.

12. Kiriya, D.; Chen, K.; Ota, H.; Lin, Y.; Zhao, P.; Yu, Z.; Ha, T.-J.; Javey, A. *J. Am. Chem. Soc.* **2014**, *136*, 11188–11194.
13. Arnold, M. S.; Green, A. A.; Hulvat, J. F.; Stupp, S. I.; Hersam, M. C. *Nat. Nanotechnol.* **2006**, *1*, 60–65.
14. Homenick, C. M.; Rousina-Webb, A.; Cheng, F.; Jakubinek, M. B.; Malenfant, P. R. L.; Simard, B. *J. Phys. Chem. C* **2014**, *118*, 16156-16164.
15. M. Zheng and E. D. Semke, *J. Am. Chem. Soc.* **2007**, *129*, 6084–6085.
16. Liu, H.; Nishide, D.; Tanaka, T.; Kataura, H. *Nat. Commun.* **2011**, *2*, 309.
17. Tulevski, G. S.; Franklin, A. D.; Afzali, A. *ACS Nano* **2013**, *7*, 2971–2976.
18. Khripin, C. Y.; Fagan, J. A.; Zheng, M. *J. Am. Chem. Soc.* **2013**, *135*, 6822-6825.
19. Fagan, J. A.; Haroz, E. H.; Ihly, R.; Gui, H.; Blackburn, J. L.; Simpson, J. R.; Lam, S.; Hight Walker, A. R.; Doorn, S. K.; Zheng, M. *ACS Nano* **2015**, doi/abs/10.1021/acsnano.5b01123.
20. Gui, H.; Steit, J. K.; Fagan, J. A.; Walker, A. R. H.; Zhou, C.; Zheng, M. *Nano Lett.* **2015**, *15*, 1642-1646.
21. Nish, A.; Hwang, J.-Y.; Doig, J.; and Nicholas, R. J. *Nat. Nanotechnol.* **2007**, *2*, 640-646.
22. Ding, J.; Li, Z.; Lefebvre, J.; Cheng, C.; Dubey, G.; Zou, S.; Finnie, P.; Hrdina, A.; Scoles, L.; Lopinski, G. P.; Kingston, C. T.; Simard, B.; Patrick R. L. Malenfant, P.R.L. *Nanoscale* **2014**, *6*, 2328-2339.
23. Lee, H. W.; Yoon, Y.; Park, S.; Oh, J. H.; Hong, S.; Liyanage, L. S.; Wang, H.; Morishita, S.; Patil, N.; Park, Y. J.; Park, J. J.; Spakowitz, A.; Galli, G.; Gygi, F.; Wong, P.; Tok, J. B.-H.; Kim, J. M.; Bao, Z. *Nat. Commun.* **2011**, *2*, 541.
24. Samanta, K. S.; Fritsch, M.; Scherf, U.; Gomulya, W.; Bisri, S.Z.; Loi, M.A. *Acc. Chem. Res.* **2014**, *47*, 2446-2456.
25. Mistry, K. S.; Larsen, B. A.; Blackburn, J. L. *ACS Nano* **2013**, *7*, 2231–2239.
26. Schießl, S. P.; Fröhlich, N.; Held, M.; Gannott, F.; Schweiger, M.; Forster, M.; Scherf, U.; Zaumseil, J. *ACS Appl. Mater. Interfaces* **2015**, *7*, 682.
27. Shea, M. J.; Mehlenbacher, R. D.; Zanni, M. T.; Arnold, M. S. *J. Phys. Chem. Lett.* **2014**, *5*, 3742–3749.

28. Pochorovski, I.; Wang, H.; Feldblyum, J. I.; Zhang, X.; Antaris, A. L.; Bao, Z. *J. Am. Chem. Soc.* **2015**, *137*, 4328-4331.
29. Toshimitsu, F.; Nakashima, N. *Nat. Commun.* **2014**, *5*:5041 | DOI: 10.1038/ncomms6041.
30. Li, Z.; Ding, J.; Finnie, P.; Lefebvre, J.; Cheng, F.; Kingston, C. T.; Malenfant, P. R. L. *Nano Res.* **2015**, DOI 10.1007/s12274-015-0725-y.
31. Kim, K. S.; Cota-Sanchez, G.; Kingston, C. T.; Imris, M.; Simard; B. Soucy, G. *J. Phys. D* **2007**, *40*, 2375–2387.
32. Finnie, P.; Ding, J.; Li, Z.; Kingston C. T. *J. Phys. Chem. C* **2014**, *118*, 30127–30138.
33. Lustig, S. R.; Jagota, A.; Khripin, C.; Zheng, M. *J. Phys. Chem. B*, **2005**, *109*, 2559-2566.
34. Wang, H.; Hsieh, B.; Jimenez-Oses, G.; Liu, P.; Tassone, C. J. ; Diao, Y. ; Lei, T. ; Houk, K. N. ; Bao, Z. *Small* **2015**, *11*, 126-133.
35. Krupke, R., Hennrich, F.; Löhneysen, H. V.; Kappes, M. M. *Science* **2003**, **301**, 344-347.
36. Blum, C.; Stürzl, N.; Hennrich, F.; Lebedkin, S.; Heeg, S.; Dumlich, H.; Reich, S.; Kappes, M. M. *ACS Nano* **2011**, *5*, 2847-2854.
37. Li, Z.; Ding, J.; Lefebvre, J.; Malenfant, P. R. L. *Org. Elect.* **2015**, *26*, 15-19.